

## RESEARCH ARTICLE

10.1002/2014JB010990

## Key Points:

- Processes in the mud volcano are the source of harmonic waveforms or tremors
- Harmonic tremors occur in swarms with a periodicity of 6 h
- Activity of the Håkon Mosby mud volcano is not affected by earthquakes

## Correspondence to:

P. Franek,  
peter.franek@uit.no

## Citation:

Franek, P., J. Mienert, S. Buenz, and L. Géli (2014), Character of seismic motion at a location of a gas hydrate-bearing mud volcano on the SW Barents Sea margin, *J. Geophys. Res. Solid Earth*, 119, 6159–6177, doi:10.1002/2014JB010990.

Received 28 JAN 2014

Accepted 5 JUL 2014

Accepted article online 9 JUL 2014

Published online 14 AUG 2014

## Character of seismic motion at a location of a gas hydrate-bearing mud volcano on the SW Barents Sea margin

Peter Franek<sup>1</sup>, Jürgen Mienert<sup>1</sup>, Stefan Buenz<sup>1</sup>, and Louis Géli<sup>2</sup>

<sup>1</sup>CAGE—Centre for Arctic Gas Hydrate, Environment and Climate, Department of Geology, UiT The Arctic University of Norway, Tromsø, Norway, <sup>2</sup>Marine Geosciences Department, Ifremer, Plouzané, France

**Abstract** The Håkon Mosby mud volcano (HMMV) at 1270 m water depth on the SW Barents Sea slope has been intensively studied since its discovery in 1989. A variety of sensors monitored morphological, hydrological, geochemical, and biological parameters in the HMMV area. An ocean bottom seismometer deployment allowed us to register seismic motion for 2 years, from October 2008 to October 2010. The analysis of seismic records documents two types of seismic signals. The first type are harmonic tremors with frequency peaks around 4–5 and 8–10 Hz that occur in swarms. Their origin could be from fluid flow circulation or resonant vibrations of gas bubbles or from delayed movement of fluid-rich sediments in the conduit or in a deeper pseudo-mud chamber of the HMMV. Because swarms occur with a periodicity of ~6 h, tide-related effects are suspected to influence the mechanism originating the tremors. The second type of signals are regional earthquakes that were in 15 cases recognized in seismic records. The activity of harmonic tremors was not significantly affected by earthquakes.

### 1. Introduction

One of the Earth's phenomena, still not fully understood in detail, is mud volcanism [Kopf, 2002]. Mud volcanos most often form positive surface expressions, so-called mounds, with geometries varying from few meters to kilometers in diameter and from 1 m to hundred meters in height and can be found onshore and offshore in many tectonic and sedimentary settings on Earth [e.g., Niemann and Boetius, 2010; Tinivella and Giustiniani, 2012]. Processes that govern mud volcanism often differ from one case to another, and there is a great diversity of mechanisms proposed to build mud volcanos. In contrast to magmatic or “hot” volcanos, mud volcanos are formed by mud discharge that is usually accompanied by fluid and gas transfer originating from deep subsurface geological layers. As such, mud volcanoes often extend to great subsurface depths forming focused fluid flow structures through deep sedimentary basins [e.g., Hjelstuen et al., 1999].

Mud volcanos are usually related to regional compressive stresses. Compression may be caused by folding, faulting, or high lithostatic loads caused by fast burial of sediments due to slope failures or high sedimentation rates [e.g., Milkov, 2000; Deville et al., 2003; Huguen et al., 2004]. All of these conditions can lead to the development of abnormally high pore fluid pressure in sediments when pore fluid pressure exceeds the hydrostatic pressure [Dimitrov, 2002; Kopf, 2002]. Buried sediments can ascend when their density is lower than the density of surrounding and overlaying material. Buoyancy contrasts in materials can result from grain density contrast with a lower density in deeper deposits or from lateral influx of fluids. The overpressurized sediment material can become fluidized and remobilizes. The remobilized sediment may rise upward through weakness zones such as faults or create vertical conduits by natural hydraulic fracturing. During the ascent, gas effervesces due to the decrease of pressure [Manga et al., 2009; Tinivella and Giustiniani, 2012]. Mud volcanos are thus emitters of mud, fluids, and gases either continuously or in regular or irregular time intervals.

Stochastic processes like earthquakes can influence fluid pressure enough to result in the triggering of mud volcano eruptions [Manga et al., 2009]. Earthquakes can also affect gas reservoirs beneath impermeable, usually gas hydrate-bearing sediments, by opening new pathways for gas and fluids making the overlaying sediments susceptible to mechanical failure [Halbach et al., 2004; Fischer et al., 2013]. Enhanced gas seepage can occur after earthquakes [Field and Jennings, 1987; Rudolph and Manga, 2012], although the effects of earthquakes on temporal variability of intensity of gas fluxes is still unclear [Lapham et al., 2013]. In addition to dynamic loading of geological layers due to earthquakes, gas pressure may also build up over time,

independent of earthquakes, resulting in fracturing of the overburden causing fluids to migrate vertically [Flemings *et al.*, 2003; Hornbach *et al.*, 2004].

The study of submarine mud volcanos received increased interest in the last decades as their presence might be linked to deep-seated petroleum systems [Milkov, 2000; Dimitrov, 2002; Albarello *et al.*, 2012]. Thus, they may indicate potential windows to deeper hydrocarbon resources [e.g., Planke *et al.*, 2003; Milkov, 2005].

The Håkon Mosby Mud Volcano (HMMV) is a prominent seafloor feature off northern Norway. Situated on the Barents Sea continental slope, a passive margin setting, it was discovered in 1989 as a feature on side scan sonar data [Vogt *et al.*, 1997]. Since its discovery, it was the target of numerous research cruises focusing on the study of its morphology, geological setting, geochemical characteristics, and chemosynthetic ecosystem. Data from acoustic profiles, in situ temperature measurements, gravity, and piston cores were collected, samples of hydrates were recovered, and video and photo surveys of the seafloor were performed [Vogt *et al.*, 1997; Hjelstuen *et al.*, 1999; Milkov *et al.*, 2004; Beyer *et al.*, 2005; Niemann *et al.*, 2006; Sauter *et al.*, 2006; Jerosch *et al.*, 2007; Feseker *et al.*, 2008; Foucher *et al.*, 2009; Pape *et al.*, 2011].

The LOOME project (long-term observations on mud volcano eruptions), a European Seas Observatory Network demonstration mission, performed long-term observations and measurements of a range of parameters at the location of the HMMV. In addition to other instruments, an ocean bottom seismometer (OBS) was deployed on the HMMV to monitor seismic activity [Mienert *et al.*, 2009]. Seismic motion over a period of 2 years (October 2008 to October 2010) was recorded in order to identify seismic signals resulting from the expulsion of mud, fluids, and gas from the HMMV and to better understand the duration, frequency, and recurrence of expulsion events and their geological controls.

## 2. Structural Setting

The HMMV is located at the Norwegian-Barents-Svalbard continental margin [Vogt *et al.*, 1997; Hjelstuen *et al.*, 1999; Perez-Garcia *et al.*, 2009] between Norway and Svalbard (Figure 1a). It is a circular structure about 1 km wide and 10 m high and lies at 1270 m water depth (Figure 1b). It is situated at the center of the Bear Island Slide scar on the SW Barents Sea slope. Based on high-resolution microbathymetric data, Jerosch *et al.* [2007] identified and quantified three morphological units of the HMMV on the seafloor. A flat area with very low relief in the central part of the mud volcano, which is denoted as Unit I, was formed by recent mud flows. A hummocky peripheral rim, Unit II, encloses the central part. A 2 m deep moat area includes a circular outcrop that constitutes Unit III, which is surrounding the mud volcano. Units I and II are considered to be the most active regions of the HMMV where chemosynthetic communities, bacterial mats, mud flows, enhanced geothermal gradients, high methane concentration in sediments, seepage bubbles, and gas hydrates were observed [Vogt *et al.*, 1997; Hjelstuen *et al.*, 1999; Niemann *et al.*, 2006; Jerosch *et al.*, 2007; Feseker *et al.*, 2008; Pape *et al.*, 2011].

The HMMV is underlain by a more than 6 km thick sequence of Cenozoic sediments [Hjelstuen *et al.*, 1999]. A 3 km thick glacial unit overlays preglacial sediments formed during a period of glaciations with high sedimentation rates, over 1000 m/Myr, [Vogt *et al.*, 1997]. Hjelstuen *et al.* [1999] relate the presence of disturbed zones in subhorizontal reflections within the glacial sediments to the presence of free gas. Perez-Garcia *et al.* [2009] interpreted the internal structure and proposed the following conceptual model for the evolution of the HMMV. During an initial period, development of overpressure in gas-rich hemipelagic sediments in the preglacial units caused hydrofracturing at the base of the glacial unit. Then rapid upward migration, mainly of gas, created a 3 km long conduit. It caused uplifting of the paleoseafloor followed by a collapse that formed the crater. The extruded mud and material from sidewalls filled the crater. The deposition of several glacial debris flows sealed the original crater and created a pseudo-mud chamber. The pseudo-mud chamber is localized approximately 300 m below the present seafloor, and its existence is evident from reflection seismic data [Perez-Garcia *et al.*, 2009]. Continuous inflow of gas into the dynamic chamber during the inactive phase decreases the density inside the pseudo-mud chamber. The decrease of the density increases the buoyancy reactivating the HMMV and creates continuation of the conduit which is terminated by a crater on the seafloor (Figure 1c).

## 3. Data Acquisition and Processing

The operational period of the OBS deployed at the HMMV location (Figure 1b) spans from October 2008 to October 2010. In July 2009, after 9 months of operation, the recovered OBS showed continuous data

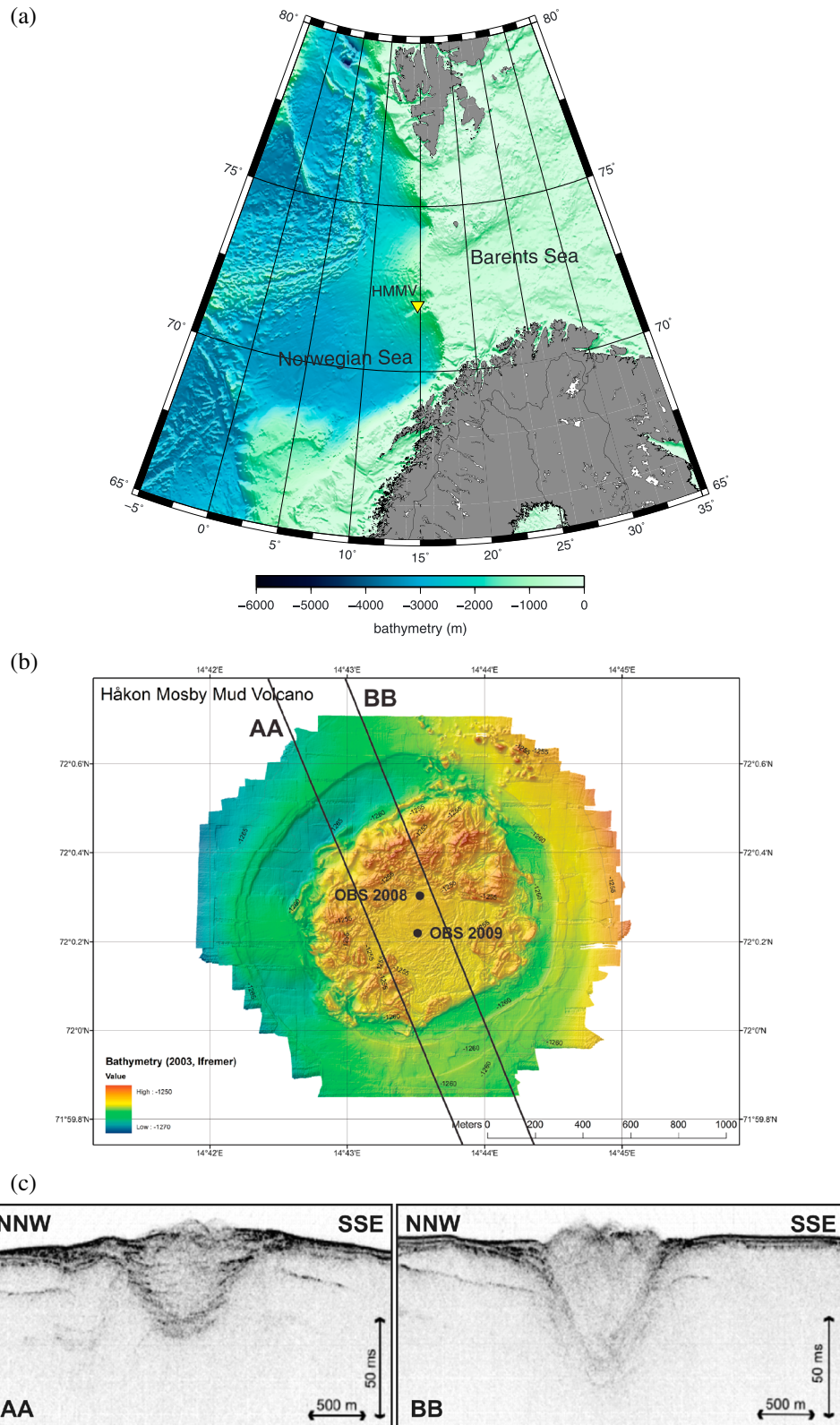


**Figure 1.** (a) The HMMV location on the Barents Sea slope between Norway and Svalbard. (b) Microbathymetry of the HMMV compiled by IFREMER (French Research Institute for Exploitation of the Sea) in 2003 [Edy *et al.*, 2004, modified]. Positions of our two deployments of the ocean bottom seismometer (OBS) station are indicated by black dots. (c) NNW-SSE oriented sediment echosounder profiles across the HMMV [from Perez-Garcia *et al.*, 2009], which locations are indicated in Figure 1b by black lines.

recording. The system was then redeployed and recovered at the end of the 2 years monitoring period in October 2010.

The OBS system consists of a titanium frame with floatation units made of syntactic foam, an acoustic release system, and a separate titanium pressure cylinder (KUM, [http://www.kum-kiel.de/eng/index\\_eng.html](http://www.kum-kiel.de/eng/index_eng.html)). Inside the cylinder, a data logger powered by lithium battery packs continuously recorded data (SEND, <http://www.send.de>). The OBS system was further equipped with a hydrophone fixed to the frame approximately 0.5 m above the seafloor and a three-component seismometer with a 4.5 Hz corner frequency. The seismometer measures ground acceleration and is mechanically decoupled from the frame in order to achieve better coupling to the seafloor and to minimize seismic noise generated by the frame. The OBS operated in continuous recording mode with a rate of 50 samples per second producing 16 bits signed digital data. Due to unknown transfer function of the seismometer, seismic records are not corrected for the instrument response. The actual orientations of horizontal components of seismic motion are not determined; hereafter, they are referred as horizontal components 1 and 2. The hydrophone records exhibit very high level of noise and often are clipped.

Data analysis includes visual examination of all three seismometer components and the hydrophone record and identification of waveforms with a signal-to-noise ratio of at least 3. We determined the Fourier amplitude spectra and spectrograms of the records. To calculate spectrograms we use a short-time Fourier transform, which allows to interpret a Fourier spectrum of a signal cut out by a sliding time window [e.g., *Bartosch and Seidl, 1999*].

For the purpose of investigating daily fluctuations of signal-to-noise ratio, records are divided into two groups, the first one with background noise and the second one with identified waveforms. For each group we have chosen 1 h part corresponding to the hour of the day, and on this segment of the seismic record we used a sliding time window with 50% overlap. Afterward, we removed from the records in every time window the mean value and slope, a Hanning taper is applied, and Fourier amplitude spectrum is calculated. The obtained spectra ensemble is used to determine the median spectrum for the chosen hour of the day.

The amplitudes of tides are modeled by MATLAB-based version of TPXO7.1, a global model of ocean tides [*Egbert and Erofeeva, 2002*].

A Schuster test and Schuster spectra are used to statistically analyze interevent times in the occurrence of swarm tremors. A detailed description of the method can be found in *Ader and Avouac [2013, and in references therein]*. For the investigated period (interevent time) we evaluate the Schuster  $p$  value, which represents the significance level to reject the null hypothesis that the occurrences of swarms are distributed randomly. The lower the  $p$  value, the higher the probability that the distribution shows periodicity.

An earthquake catalogue was compiled from a broader area from 30°W to 45°E and from 55°N to 86°N containing earthquake events that occurred during the operational period of the OBS station. Parameters of the earthquakes (location, hypodepth, origin time, and magnitude) are extracted from online available bulletins—from the International Seismic Center (Reference Event Bulletin, <http://www.isc.ac.uk>), the Incorporated Research Institutions for Seismology (<http://www.iris.ed>), the European-Mediterranean Seismological Centre (<http://www.emsc-csem.org>), and from the NORSAR regional reviewed bulletin (<http://www.norsardata.no/NDC/bulletins/regional>). The compiled data were reviewed and duplicate events removed. To estimate the expected arrival times of seismic waves of earthquakes to the HMMV location, we use tables of traveltimes of  $P$  and  $S$  waves from the iasp91 model [*Kennett and Engdahl, 1991*], and for the speed of  $T$  waves we use 1.5 km/s.

#### 4. Results

After the overall visual inspection of 2 year records, we identified several characteristic signals. The records are dominated by a very large number of waveforms with harmonic content (Figure 2a). Similar harmonic waveforms appear in the seismic records of tremors of magmatic volcanos [*Konstantinou and Schlindwein, 2002; Ripepe et al., 2010*]. Those seismic signals are generated in various parts of a magma-filled conduit and create interference patterns [e.g., *Neuberg, 2000*]. Hence, for the harmonic waveforms in our seismic records we use the term harmonic tremors or tremors.

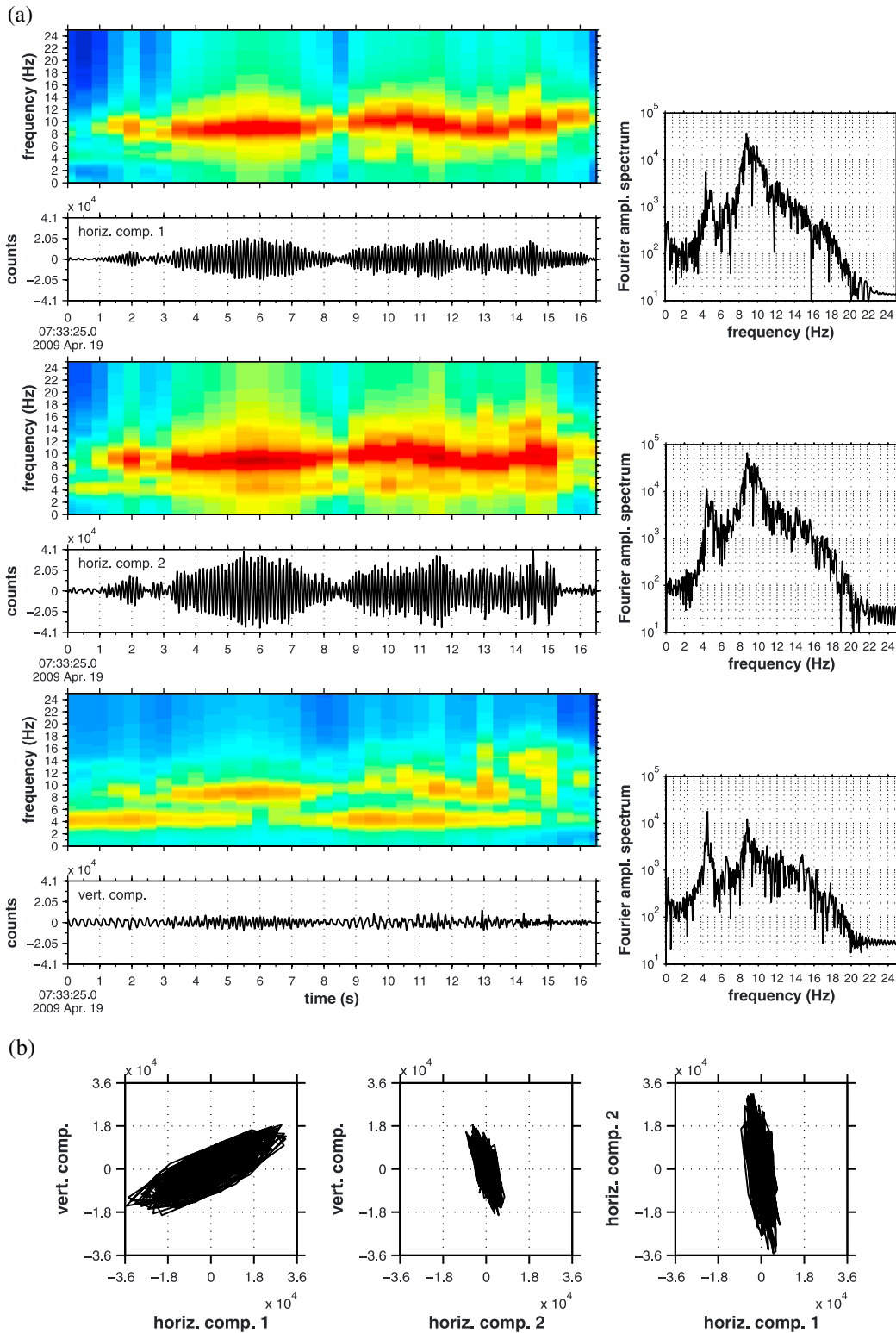


**Figure 2.** (a) Record of vertical and horizontal components 1 and 2 of harmonic tremor, their spectrograms, and Fourier amplitude spectra. Starting time of records correspond to 19 April 2009, 07:33:25.0. Spectrograms are logarithmically scaled from minimum value of logarithm of amplitude (0.8) to maximum value (4.2), where blue color corresponds to minimum and red to maximum. Spectrograms were calculated by sliding time windows of 1.0 s duration and 0.5 s overlap. Note the frequency peaks at ~4.5 Hz and 9 Hz for all components of seismic motion and their variation during tremor. (b) Particle motion of harmonic tremor from Figure 2a that was filtered with band-pass Butterworth filter in the frequency range 2–10 Hz. Shown is particle motion in two vertical planes (vertical versus horizontal comp. 1, vertical versus horizontal comp. 2) and in a horizontal plane (horizontal comp. 2 versus horizontal comp. 1).

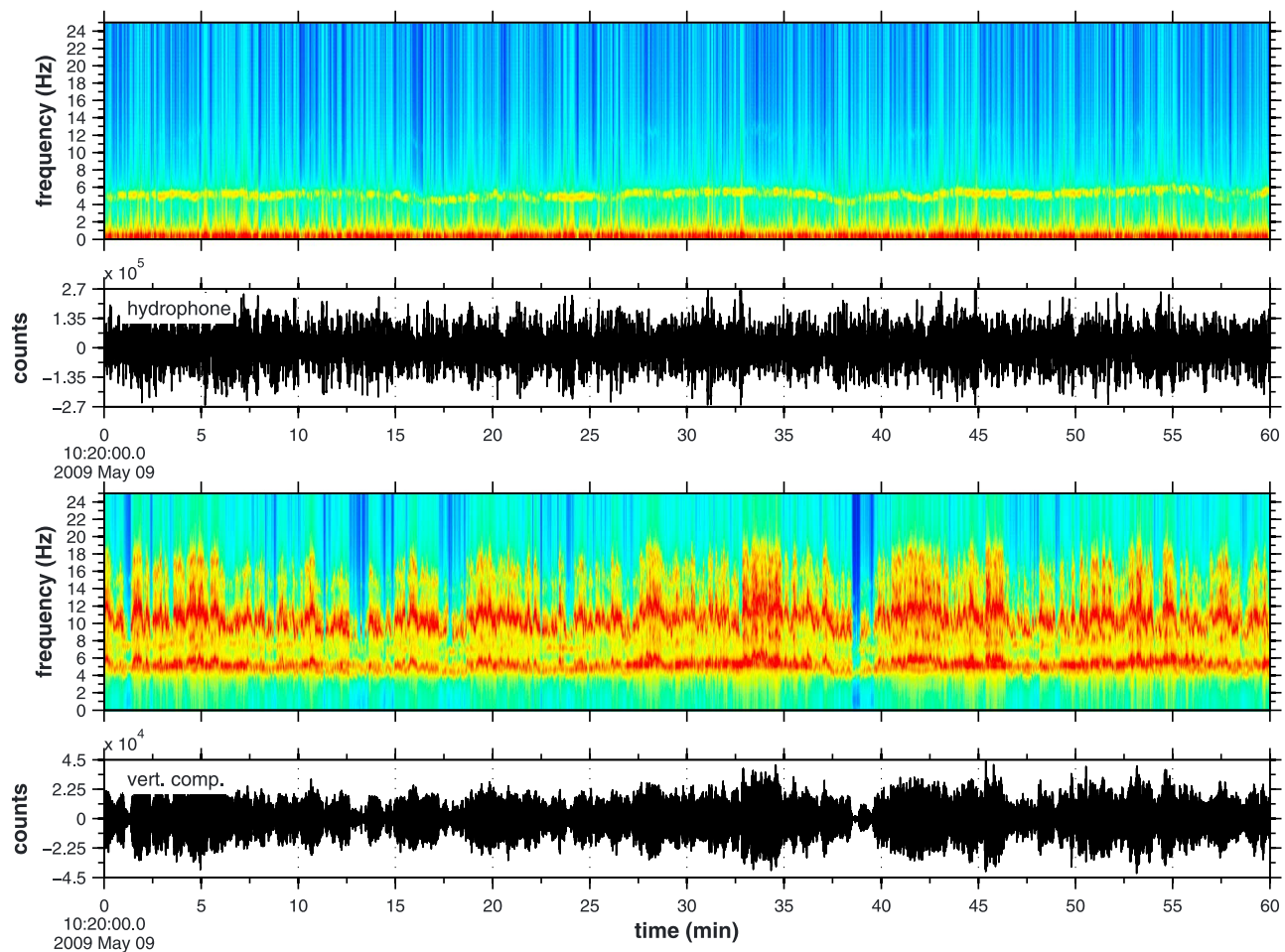


**Figure 3.** Hydrophone record and record of vertical component and their spectrograms. Starting time of records correspond to 9 May 2009, 10:20:00.0. Spectrograms of hydrophone record and vertical component are logarithmically scaled from minimum value of logarithm of amplitude (1.9 for hydrophone record and 0.6 for vertical component) to maximum value (5.3 for hydrophone record and 4.1 for vertical component), where blue color corresponds to minimum and red to maximum. Spectrograms were calculated by sliding time windows of 3.0 s duration and 1.5 s overlap.

Among the signals associated with the tremor swarms, we also noticed in the records signals that most probably correspond to earthquakes. Their analysis is summarized in Appendix A.

#### 4.1. Harmonic Tremors

We identified harmonic tremors by visual inspection of all three components of seismic motion and their spectrograms. Their amplitudes have a wide range of values and are well above the level of noise. Frequency peaks are consistently occurring at  $\sim 4\text{--}5$  Hz and  $8\text{--}10$  Hz, with slight variation toward higher and lower frequencies during the tremor duration. Low-frequency peaks are usually more dominant in the case of vertical motion; peaks at higher frequencies are more pronounced on horizontal components. In some cases we observe frequency peaks occurring in the range of  $11\text{--}13$  Hz. It may suggest that frequency peaks are the multiples of basic resonant mode with frequency  $4\text{--}5$  Hz.

Polarization analysis of all harmonic tremors is quite challenging, given their very frequent occurrence. To have some insight we have randomly picked up one harmonic tremor per every week of the recording period, and for these tremors we performed polarization analysis. Particle motion diagrams of the tremors from the first OBS deployment reveal stable linear movement in the horizontal and in both vertical planes (Figure 2b). Tremors from the second deployment display also linear movement in all three planes; however, the orientation varies with time, and irregular movements occur. This change in polarization can be attributed to different location of the OBS in the first and the second OBS deployment.

Harmonic tremors are clearly recorded on all three components of seismic motion (Figure 2a) but do not appear in the hydrophone records. However, in several cases we observe weak frequency peaks in the same frequency range as in the case of vertical component, but the high level of noise limits the potential for interpretation (Figure 3).

The duration of tremors is from several seconds to tens of seconds. Occurrence of tremors is not uniform, and they usually occur in swarms. Tremor swarms last from few minutes up to several hours, and in some cases they lasted days (Figure 4a). Their average duration is 6.7 h. Overview of the tremor swarms activity is provided in Figure 4c, where the total number of hours of tremors per day during the whole period of the OBS deployment is shown. Tremor swarms occur almost everyday, and the more active days are alternated by the intervals of relative quiescence. From the occurrences of tremor swarms we determined the interevent times, which we calculated as the difference between onset times of two successive swarms. The average of interevent times is 13.7 h. A histogram shows the distribution of the number of swarms relative to the interevent times (Figure 5a). It documents two local maxima, a high peak at  $\sim 12$  and much smaller peak at  $\sim 25$  h.

Figure 5b shows the median spectrum of background noise and tremor swarms as a function of hour of the day. Spectra are calculated by applying 1 min sliding time window. We computed median spectra for various lengths of sliding time windows, and in all cases the level of noise and tremor swarms was not changing during the day. We note that the noise spectrum is remarkably stable. Therefore, we conclude that peaks in the distribution of swarms are not related to daily fluctuations of the signal-to-noise ratio.

To reveal if the occurrence of tremor swarms is actually periodic, we computed a Schuster spectrum (Figure 5c). *Ader and Avouac* [2013] estimated a threshold for  $p$  values below which it is possible to consider with confidence periodicity in the data. The  $p$  value that is below 5% of this expected value corresponds to the detection of periodicity with more than 95% confidence. In our case there is only one such  $p$  value and it occurs at 6.2 h. It is also possible to notice a group of  $p$  values around a period of 12 h; however, none of them is below the expected threshold value.

Two peaks in the histogram (Figure 5a) and an approximate 6 h period of the occurrence of tremor swarms (Figure 5c) may suggest a correlation with tides. We calculated the time difference between the onset of tremor swarms and the nearest amplitude maximum of the modeled tide that preceded the swarm. Figure 6a shows the time differences (time delays) for the whole 2 year period of the OBS deployment. If the swarm occurrence is governed mainly by tides, the distribution of time delays would be clustered along a horizontal line. Apparently, the distribution in Figure 6a does not exhibit any clustering. Nevertheless, the histogram for time delays (Figure 6b) indicates a presence of two small maxima at about 4 and 11 h, and the sinusoidal function fits the distribution of a period of 6.4 h.

#### 4.2. Short-Duration Events

The seismic records also show a large number of events of very short duration less than 1 s (Figure 7). A STA/LTA (short-time average/long-time average) algorithm was applied for automatic recognition of these events, but the method did not detect numerous short-duration events and detected a considerable number of non-short-duration events. The large number of missed or false triggers is probably due to the presence of harmonic tremors. They frequently overlap short-duration events, thus making visual identification difficult and erroneous. For this reason we did not systematically analyze them. However, based on the analysis of several short-duration events, it appears that they have the frequency content in a range from 3 to 20 Hz with one or several frequency peaks, variable amplitudes, and do not show secondary arrivals that could be identified as S waves.

#### 4.3. Sediment Movement

During the second deployment of the OBS (July 2009 to October 2010) on 27 September 2009, a massive uplift of the seafloor followed by deflation took place, disturbing the mud volcano surface (T. Feseker, personal communication, 2013). Noteworthy, at the time of this event we did not recognize any increased activity in the seismometer or hydrophone records when compared to other days with tremor swarms (Figure 4). However, the number and amplitudes of tremors decreased several days before and after this event. It is not evident how fast the event occurred. Since there is no obvious activity in our seismic data, we

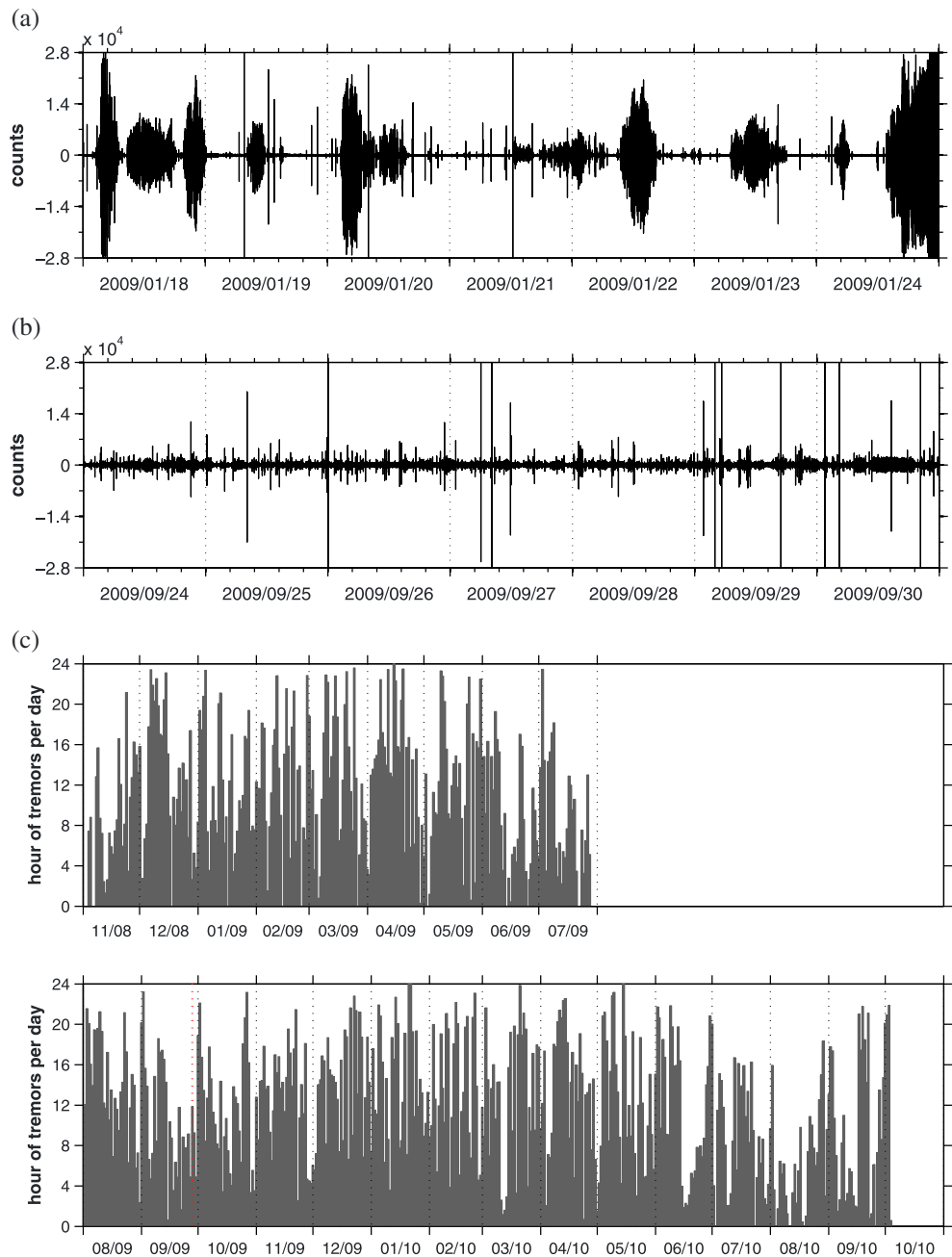


**Figure 4.** Seven days record of vertical component of (a) seismic motion with “regular” tremor swarms from January 2009 and (b) seismic motion with the disturbance of the mud volcano surface that occurred on 27 September 2009. (c) Total number of hours of tremors per day during the 2 year period of the OBS deployment. Red dotted line corresponds to 27 September 2009.

assume that the mud flow event was a relatively slow movement of sediments. Thus, only very low frequency vibrations were generated, and those would have been out of the frequency range of the seismometer.

## 5. Discussion

### 5.1. Origin of Harmonic Tremors

The harmonic character of the tremors recorded in 2 years of our OBS deployment suggests that this type of signal is due to seismic noise. In the following, we discuss several sources that generate harmonic signals that could explain tremors recorded at the HMMV location.

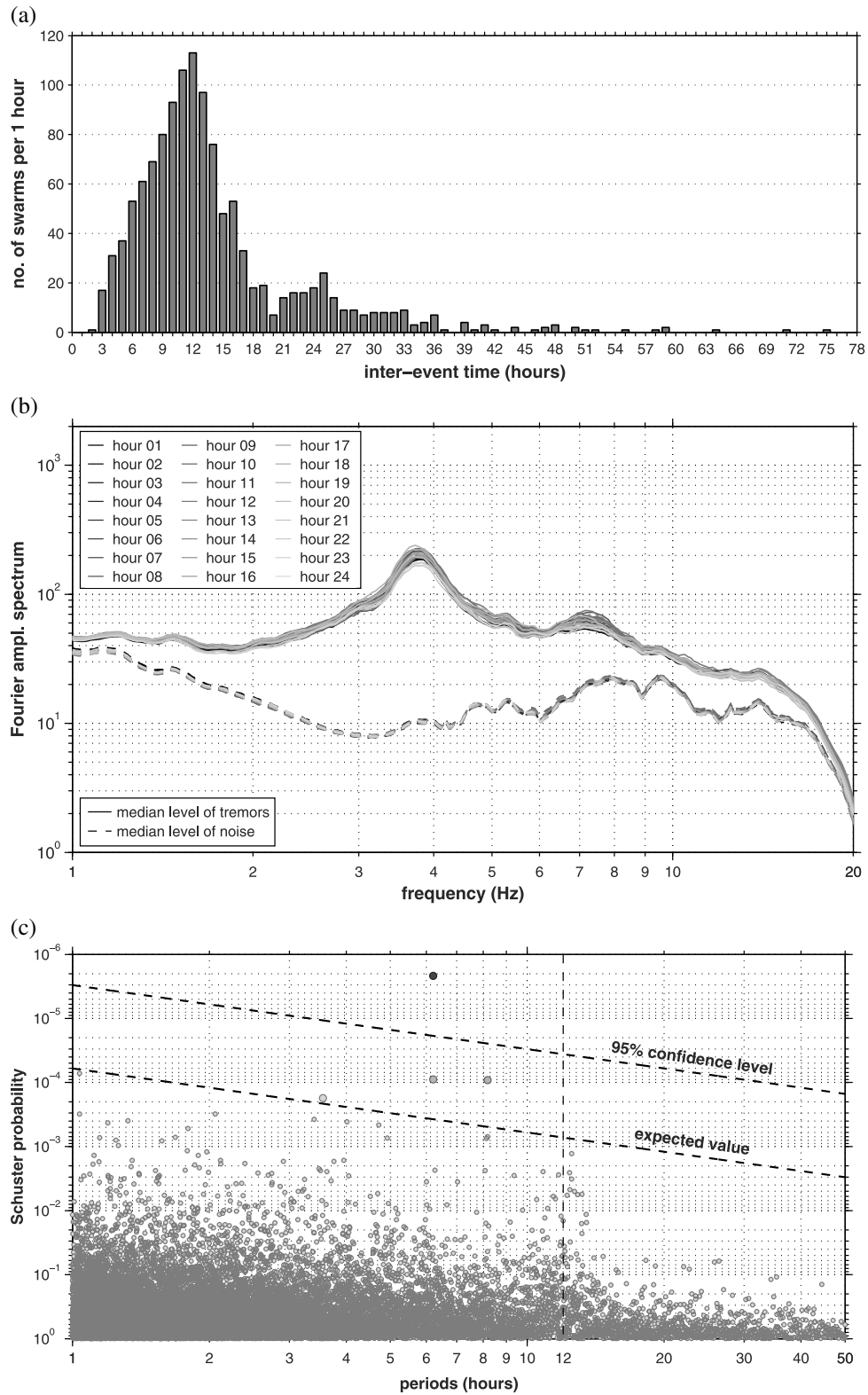


**Figure 5.** (a) Distribution of number of tremors occurring in swarms per 1 h relative to interevent time, with two local maxima at 12 and 25 h. (b) Median spectra of background noise (dashed lines) and tremor swarms (solid lines) as a function of hour of the day determined from vertical component of motion. Hour of the day is represented by color of spectrum from full black (hour 1) to light grey (hour 24). Spectra are calculated by applying 1 min sliding time window. (c) Schuster spectrum calculated for the occurrence of swarm tremors. Only one  $p$  value (Schuster probability) at 6.2 h period is below 5% of the expected value that corresponds to 95% confidence level. Note the reversed orientation of  $y$  axis.

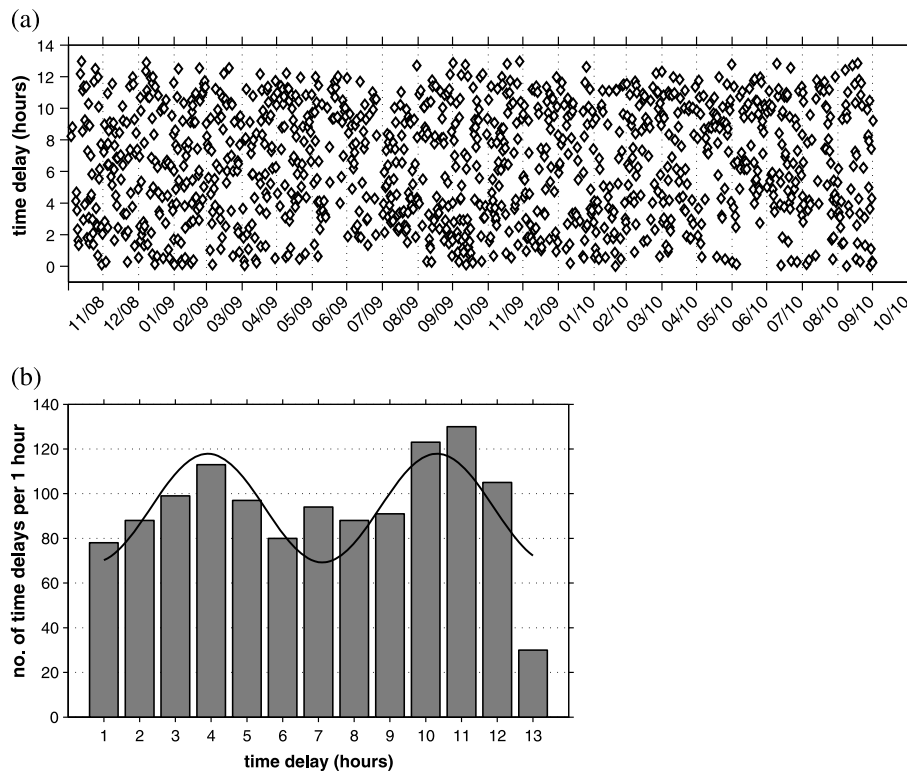


**Figure 6.** (a) Time delays of the beginning of tremor swarms relative to the nearest preceding amplitude maximum of ocean tides. Ocean tides were modeled by MATLAB-based version of TPXO7.1, a global model of ocean tides, at the HMMV location. (b) Distribution of number of time delays per 1 h relative to time, with two small maxima at about 4 and 11 h. Solid curve is sinusoidal function fitted to the distribution and has period of 6.4 h.

*Signals from seismic surveys.* Tremors in the records of this study occur during the whole 2 year period of the OBS deployment. Tremors do not exhibit the repeating burst-like pattern from shots associated with seismic surveys, and their frequencies are atypical for seismic surveys.

*Signals from ship propellers (fishing boats, tankers, etc.).* These signals usually have distinct narrow frequency peaks that shift from higher to lower frequencies over time indicating moving objects (Doppler shift; at 10 knots speed of source this shift is about 0.3%). Time-frequency character of tremors recorded at the HMMV location does not exhibit such features.

*Faunal signals (whales).* Lowest frequency of documented acoustic signal of the blue whale has dominant frequency of 12 Hz [Pontoise and Hello, 2002], which is above the frequency peaks for the majority of tremors in our records. Time distribution of faunal signals would be also irregular and should not be periodic. Signals of biological origin do not fit the signature of recorded signals.

*Ocean gravity waves.* This is seismic noise that affects a broad range of very low frequencies and at the seafloor dominates up to 4 Hz [Olofsson, 2010], which is at the lower limit of observed frequency peaks of tremors and does not explain peaks at higher frequencies. Therefore, this type of source can be also disregarded.

*T waves.* These are waterborne seismic phases from earthquakes. When an earthquake occurs under the seafloor, part of radiated seismic energy can be transferred into the ocean and propagates as acoustic signal in the SOFAR channel (Sound Fixing and Ranging), a layer of minimum sound speed that acts as a wave guide [Okal, 2008]. *T* waves may exhibit monochromatic character [Talandier and Okal, 1996] very similar to our records. Earthquakes could be considered as a source, but comparison of predicted arrival times of *T* waves of compiled earthquakes with the occurrence of tremors did not show any significant correlation. Since the

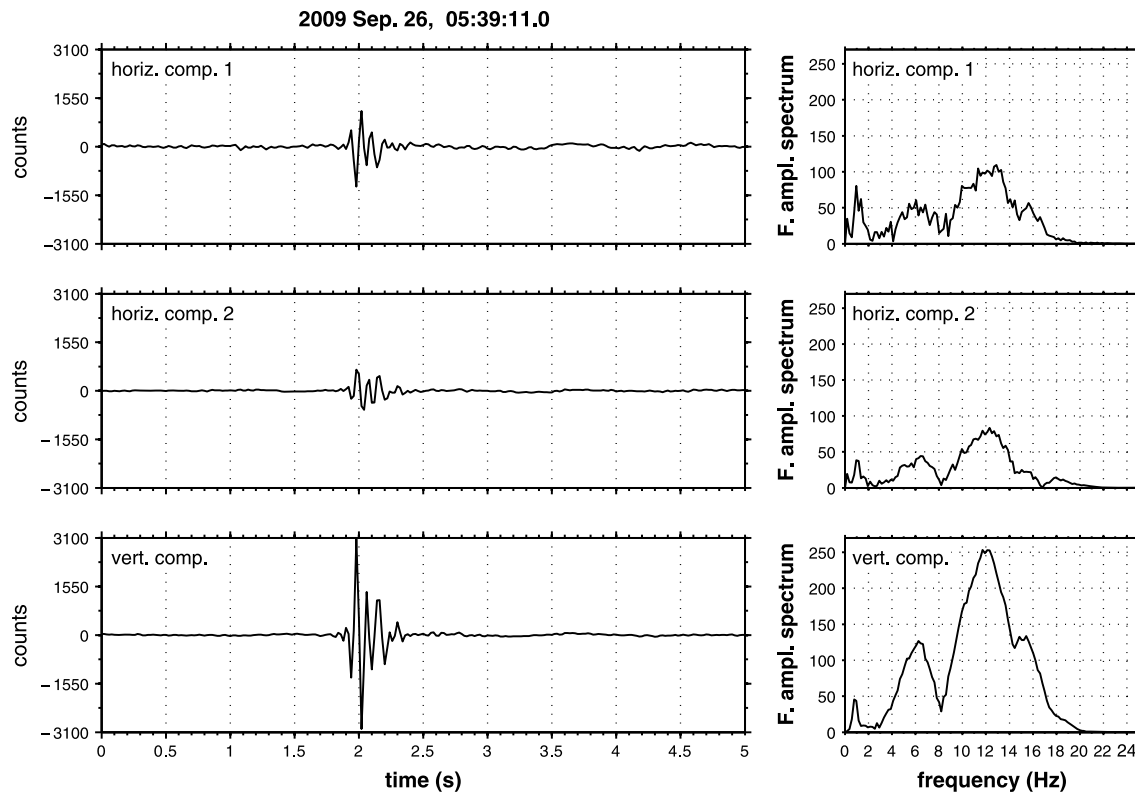


**Figure 7.** Example of short-duration event recorded on vertical and horizontal components 1 and 2 and corresponding Fourier amplitude spectra. Starting time of records is 26 September 2009, 05:39:11.0.

HMMV is not situated in a tectonically active region, the only source could be the mud volcano itself. However, *T* waves as signals propagating in water should be recorded by hydrophones on the seafloor seismic station. The inspection of our hydrophone records at the times of the occurrence of tremors did not show the presence of any notable signals except the background noise. Therefore, we do not consider *T* waves as a source for the harmonic tremors.

Olofsson [2010] reviews several types of marine ambient noise recognizable in the OBS records, including some of those we have already mentioned. Noise signals that the author denotes as *noise type 6* and *noise type 7* have the most similar characteristics to our seismic records of tremors. Olofsson assumes that the noise type 6 is due to imperfect design of recording units he had used. His recording units were equipped with a flagpole pinned to a tube with leaving small space between pole and tube. So water currents could trigger flagpole resonant vibrations that could couple into the ground as shear modes and were registered by a nearby seismic sensor. This type of noise was present in all of his three seismometer components but not in hydrophone records. When the noise occurred, it lasted from several hours to days. It had a narrow frequency band with peak frequency around 6–7 Hz. It often started at low frequency then settled at some upper value and dropped off to a low frequency before disappearing. In the records from the HMMV there is no obvious pattern of such seismic signals—our tremors have more than only one frequency peak, and we observed the occurrence of harmonic signals in hydrophone records. Therefore, Olofsson's noise type 6 most probably does not correspond to the tremors from the HMMV location.

Noise type 7 has many similar characteristics with noise type 6, but it is more similar to our records of tremors. The noise is present in all three seismometer components. Frequency peaks are not narrow and, rather, span a wider frequency range with several peaks. Olofsson attributes this type of noise to water currents which can be modulated by tides. Water currents push against the OBS unit and seafloor topography, and in this way they excite the resonances of the instrument—seafloor system.

From all previously mentioned sources of seismic noise only Olofsson's noise type 7 seems to be the best candidate corresponding to the observed tremors at the HMMV location. However, it does not provide the

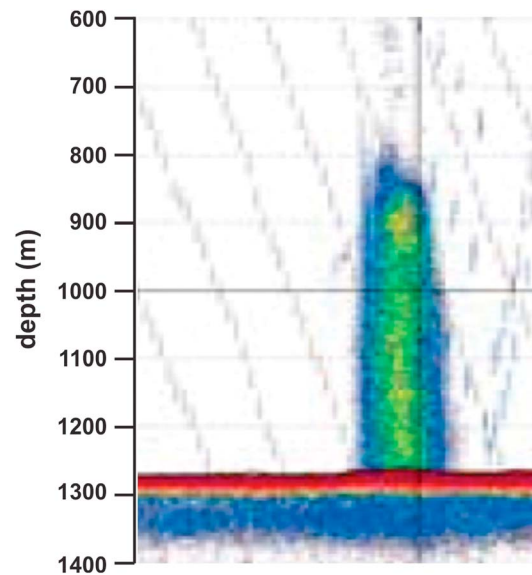


**Figure 8.** Gas plume above the HMMV (October 2008) as seen in the 18 kHz echolot. Note that the plume has a height of about 450 m but no horizontal deviations indicating weak currents during the time of the recording [from Mienert *et al.*, 2009, modified].

explanation of several weak harmonic signals observed in our hydrophone data and the rather uniform distribution of time delays between tremor swarms and the maximum of the tides (see Figure 6a). Thus, we assume that tremor swarms are not due to the water currents or other seismic noise sources but originate from the inside of the mud volcano. However, we cannot rule out the existence of weak effects of water currents that are modulated by tides.

Periodic eruptive behavior [e.g., Michaut *et al.*, 2013] and the occurrence of harmonic tremors [e.g., Kasahara, 2002; Konstantinou and Schlindwein, 2002; Tolstoy *et al.*, 2002; Ripepe *et al.*, 2010] similar to those analyzed here are often observed in active regions with magmatic volcanism. A variety of physical mechanisms have been proposed to explain the origin of such tremors. These models include oscillations of large magma bodies, cracking processes, excitation and resonance of fluid-filled cracks, fluid flow-induced oscillations of conduits, and bubble oscillation due to hydrothermal boiling. The

bubbling processes are also an important behavior of the mud volcanism [Albarello *et al.*, 2012]. Occurrence of harmonic tremors is reported in areas without any volcanic activity and can be linked to gas venting [Pontoise and Hello, 2002] or to the resonant excitation in fluid-filled cracks due to hydrothermal circulation [Díaz *et al.*, 2007].

In the framework of the mechanisms mentioned above we may speculate about the possible source of harmonic tremors identified in this study. According to the model of Perez-Garcia *et al.* [2009], gas-rich muds and fluids ascend in the conduit of the mud volcano, gas effervesces, and bubbles are formed. As they ascend, they may be trapped beneath an impermeable layer of shaly mud that plugs the conduit temporarily at shallow depth or deeper in the pseudo-mud chamber. This impermeable layer might open existing fracture for gas release once pressure buildup is high enough in the trapped gas. The accumulated gas bubbles are then released and potentially gas flares observed (Figure 8). During the venting of gas bubbles resonant vibrations of their surfaces are excited [Pontoise and Hello, 2002; Albarello *et al.*, 2012]. Small distances between bubbles and their large number create bubble clouds that enable them to behave as coupled oscillators, where coupling is provided by mutual hydrodynamic and acoustic interaction [Pontoise and Hello, 2002]. Resonant vibrations of the coupled oscillators are transmitted into the seafloor as tremor swarms that are periodically occurring. Excitation of harmonic tremors from opening and closing fractures can also contribute.

A possible impermeable layer is the shaly mud or hydrate-bearing sediments. At the HMMV location shallow subbottom gas hydrates exist [Vogt *et al.*, 1997; Jerosch *et al.*, 2007]. Pape *et al.* [2011] estimated their distribution and thickness across the entire mud volcano. The thickness ranges between less than 1 m in the center and more than 45 m at the outer limit. For a hydrate lid we could consider the cracking due to accumulated gas that establishes pressure on the hydrate lid from below until its resistance is overcome. However, this idea of accumulated gas below a solid gas hydrate lid might be doubted because it would require relatively fast formation of hydrates to heal fractures. Further, since the thickness of hydrate layer is very small, so would the stress for cracking [Hornbach *et al.*, 2004], and small amounts of trapped free gas below hydrate lid might be not enough for formation of coupled resonant vibrations after release of gas bubbles. Moreover, a very thin or lacking gas hydrate layer in the central zone was also reported by previous studies [Vogt *et al.*, 1997; Ginsburg *et al.*, 1999; Hjelstuen *et al.*, 1999; Jerosch *et al.*, 2007]. Thus, the accumulation and release of gas bubbles from below the hydrate lid that covers top of the mud volcano seems not to be likely, and impermeable sedimentary layer is more plausible.

In this context it is also possible to understand sediment movement that took place on 27 September 2009. Accumulation of mud in the conduit was probably initiated several days before this event, and it suppressed gas migration along fractures resulting also in suppression of the associated excitation of harmonic tremors. After mobilization and relatively slow extrusion of material that was not registered by seismometer, the impermeable layer was absent. Several days were necessary for formation of the layer and to establish the conditions for exciting harmonic tremors again. Similar periods of decreased activity occur throughout 2 years of the OBS deployment (see Figure 4c) and may thus indicate episodes of sediment movement or mud eruption.

As suggested previously, gas bubbles may not be sufficient for coupled oscillations that lead to harmonic tremors. If not, then resonant excitation due to circulation of fluids in the pseudo-mud chamber and in the conduit would be the source of harmonic tremors. The 6.2 h period of occurrences of swarms and two weak maxima at 4 and 11 h in the distribution of time delays supports such a possibility (see Figures 5c and 6b). These maxima may suggest that the occurrences of tremor swarms are delayed by 4–5 h after the maximum and the minimum of the tide. Maxima and minima may drive changes in the circulation of fluids.

In either case we suppose that the sources of tremor swarms relate to the processes in the mud volcano that are affected by tides. However, it may not be the only factor that governs the occurrence of tremor swarms. Indeed, tidal changes of water level and so the pressure variations on the seabed can induce pore pressure variation in the sediments [Sultan *et al.*, 2011] that attenuates with depth and is phase shifted depending on the depth [Wang, 2000]. Compressibility of pore fluids is affected also by the gas effervescence and dissolution processes, gas accumulation, and fluid migration [Sultan *et al.*, 2011]. Coupled with the effect of tides, these processes form nonuniform variations of pore pressure at different depths resulting in varying delays of swarm occurrences to the maximum of tides. This may explain rather uniform distribution of time delays between tremor swarms and the amplitude maximum of tides.

This is in contrast with traditional gas reservoirs where tides clearly caused a change in the amount of gas released [e.g., Boles *et al.*, 2001; Torres *et al.*, 2002; Leifer and Wilson, 2007]. This contrast is also strengthened by the lack of response of the mud volcano to earthquakes. We did not notice any significant change in activity of harmonic tremors during and shortly after the recorded earthquakes. The link between earthquakes and increased gas release has been indicated for gas reservoirs [e.g., Lapham *et al.*, 2008; Fischer *et al.*, 2013], and if harmonic tremors are related to gas release or fluid circulation in the case of the HMMV, then an increase in activity might be expected.

## 5.2. Origin of Short-Duration Events

Short-duration events of the same character as short-duration events in our records were observed in areas of various tectonic and sedimentary settings (Galicia Margin—Díaz *et al.* [2007], Niger Delta—Sultan *et al.* [2011], North Anatolian Fault—Tary *et al.* [2012] and Embriaco *et al.* [2013]). In general, all these events have duration up to 1 or 2 s in the frequency range from 4 to 30 Hz with eventually one or two frequency peaks, highly variable amplitudes, and impulsive onset. They also do not show clear secondary arrivals that could be identified as S waves. The events are rarely correlated from one OBS to another with the exception of closest ones that suggests superficial or very shallow sources located in very close vicinity of the OBS in the sediments with high attenuation of seismic waves. Origin of the short-duration events was attributed to the fracturing processes as the gas migrates in the porous and saturated media at the seafloor or near subsurface [Sultan *et al.*, 2011; Tary *et al.*, 2012]. A correlation to an abrupt increase of dissolved methane concentration in the sea water was shown as well [Embriaco *et al.*, 2013].

## 6. Conclusions

In this study we analyzed seismic events recorded during a 2 year period at the location of the HMMV at ~1300 m water depth on the Barents Sea continental slope offshore Norway. The majority of the events are harmonic tremors with frequency peaks ~4–5 and 8–10 Hz. Tremors occur in swarms with a periodicity of about 6 h; however, their occurrence is not primarily controlled by tides. We suggest that the main mechanism responsible for these harmonic tremors is the fluid flow circulation in the conduit and/or pseudo-mud chamber or, alternatively, the resonant vibrations of gas bubbles that behave as coupled oscillators during the release of fluids and gases from the mud volcano.

The HMMV mud slide event on 27 September 2009 was probably a very slow movement of sediments. This movement was not accompanied by any significant tremor activity.

We recognized events of very short duration up to 1 s in the seismic records, but due to the difficulties with automatic detection, we were unable to systematically analyze this type of signal. Based on the similarity with short-duration events that were presented and analyzed in previous studies, we attributed short-duration events to the fracturing processes as the gas migrates in the porous and saturated media within the seafloor or near subsurface.

We compiled a list of earthquakes from the broader area that were likely to be registered by the OBS station. From almost 4500 events only 15 were recognized in the OBS records, either because the frequency content of seismic waves was out of the detectable range of the seismometer or because the amplitudes of seismic waves were concealed by the mud volcano activity or seismic noise. The occurrence of harmonic tremors was not significantly affected by the earthquakes.

Limited monitoring of the HMMV activity by one seismometer did not allow us to accurately localize sources but does provide the seismic information to define the characteristics of harmonic tremors. An array of several broadband seismometers could enable future studies to better identify and localize close or more distant earthquake sources and slow mud flows. Such array of seismometers in cooperation with methane sensors and bubble detectors may allow to better identify the origin of harmonic tremors, short-duration events, and/or discriminate between resonant oscillation of gas bubbles and resonant excitation due to circulation of fluids as a suggested source of harmonic tremors at the HMMV location.

### Appendix A: Analysis of Recorded Earthquakes at the HMMV Location

At the HMMV location we installed only one seismometer; thus, it was not possible to identify and localize earthquakes and/or microearthquakes reliably. Therefore, we concentrated on stronger events identified and localized by multiple networks of seismic stations as well. Figure A1a shows locations of epicenters of all compiled events consisting of 4495 earthquakes. Most of seismic activity concentrates, as anticipated, along the mid-ocean ridge-spreading systems; however, some seismic activity occurred in the region near the mud volcano.

We visually checked seismic records at the expected arrival times of *P* and *S* waves of earthquakes and were able to identify 15 earthquakes (Figure A1b). Parameters of identified earthquakes are listed in Table A1. Since most of the earthquakes compiled are either weak events or had large epicentral distance, higher-frequency content of seismic signals was quickly attenuated and only seismic waves with lower frequency content arrived at the location of the HMMV. We assume that the frequency content of these seismic waves was at least partly out of the detectability range of the seismometer. Also, seismic noise had significantly higher

**Table A1.** Parameters of Earthquakes Identified in Seismic Records of the OBS at the HMMV Location<sup>a</sup>

No.	Date <sup>b</sup>	Origin Time	Latitude	Longitude	Depth (km)	M	Distance (km)	T Wave
1	2008-11-4	02:13:00.60	73.41	14.72	0	3.0	157	yes
2	2008-11-7	21:40:57.52	71.69	-11.69	2	5.1	908	no
3	2008-12-15	20:35:32.90	70.24	22.77	0	1.2	349	no
4	2008-12-20	00:06:52.49	70.95	-7.15	10	4.2	777	yes
5	2008-12-20	19:21:21.40	71.26	13.65	0	2.5	90	yes
6	2008-12-24	16:57:09.00	67.82	20.44	2	1.0	513	no
7	2009-1-5	00:42:12.80	67.76	20.40	0	1.0	519	no
8	2009-1-12	21:08:34.00	67.70	33.76	0	1.6	866	no
9	2009-1-16	15:42:57.70	71.35	14.16	10	2.2	75	no
10	2009-1-25	15:21:01.70	71.78	15.61	10	2.0	40	yes
11	2009-1-31	15:36:24.30	72.23	15.95	10	2.5	49	no
12	2009-3-18	04:36:08.95	71.02	15.95	0	2.6	117	yes
13	2009-8-20	06:35:05.24	72.21	00.93	9.5	6.0	471	yes
14	2010-5-16	13:08:17.65	73.32	07.45	0	3.4	282	yes
15	2010-6-15	19:14:42.70	70.27	12.96	2	4.2	202	yes

<sup>a</sup>Last column indicates the record of observed earthquakes with arrival of late wave train corresponding to *T* phase of seismic waves.

<sup>b</sup>Dates are formatted as year-month-day.

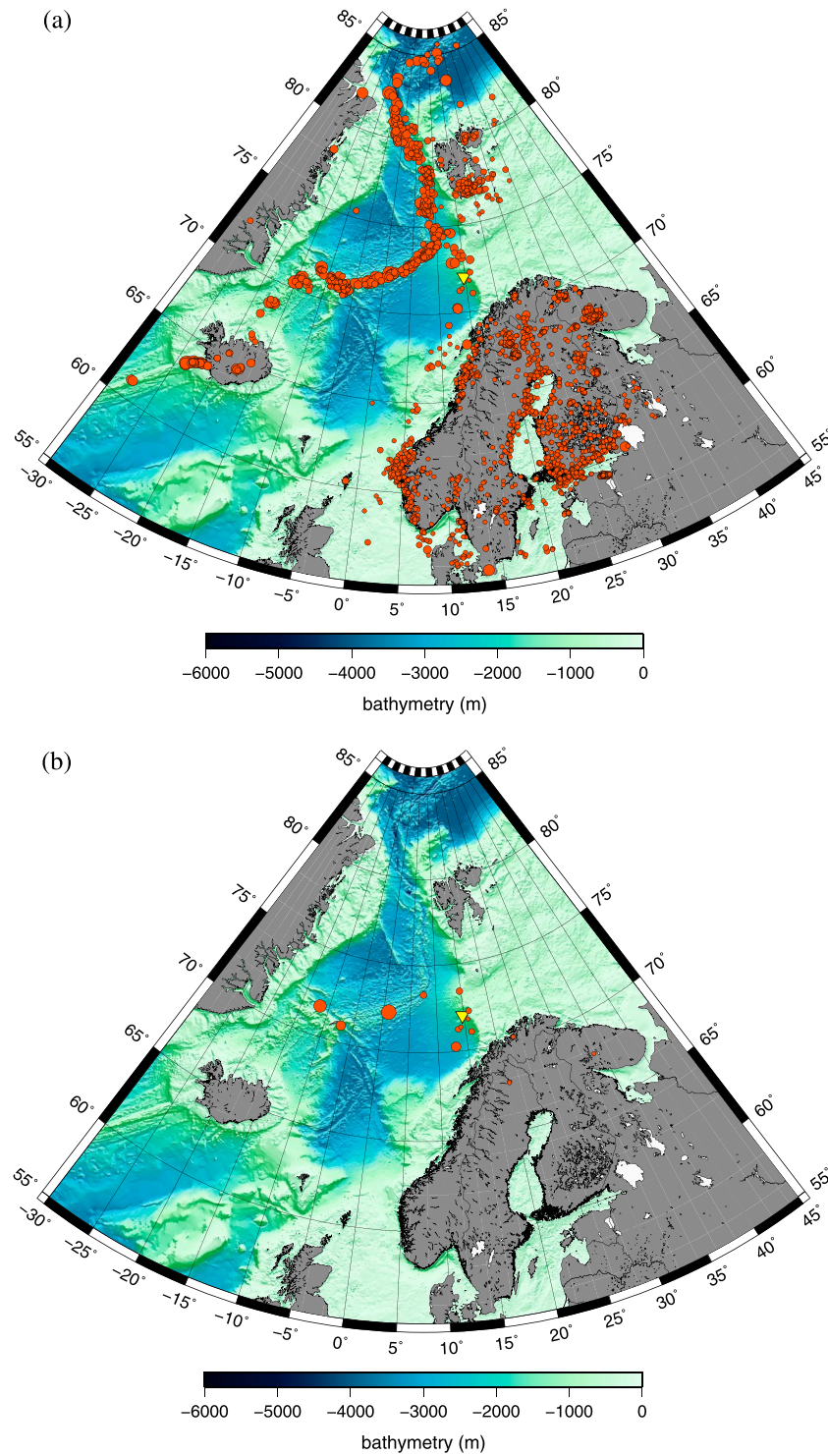


**Figure A1.** (a) Earthquake epicenters listed in the compiled events for the operational period of the OBS from November 2008 to October 2010 (red circles with size scaled to the magnitude of events). The HMMV location is indicated by yellow triangle. (b) Earthquake epicenters that were identified in the seismic records of the OBS.

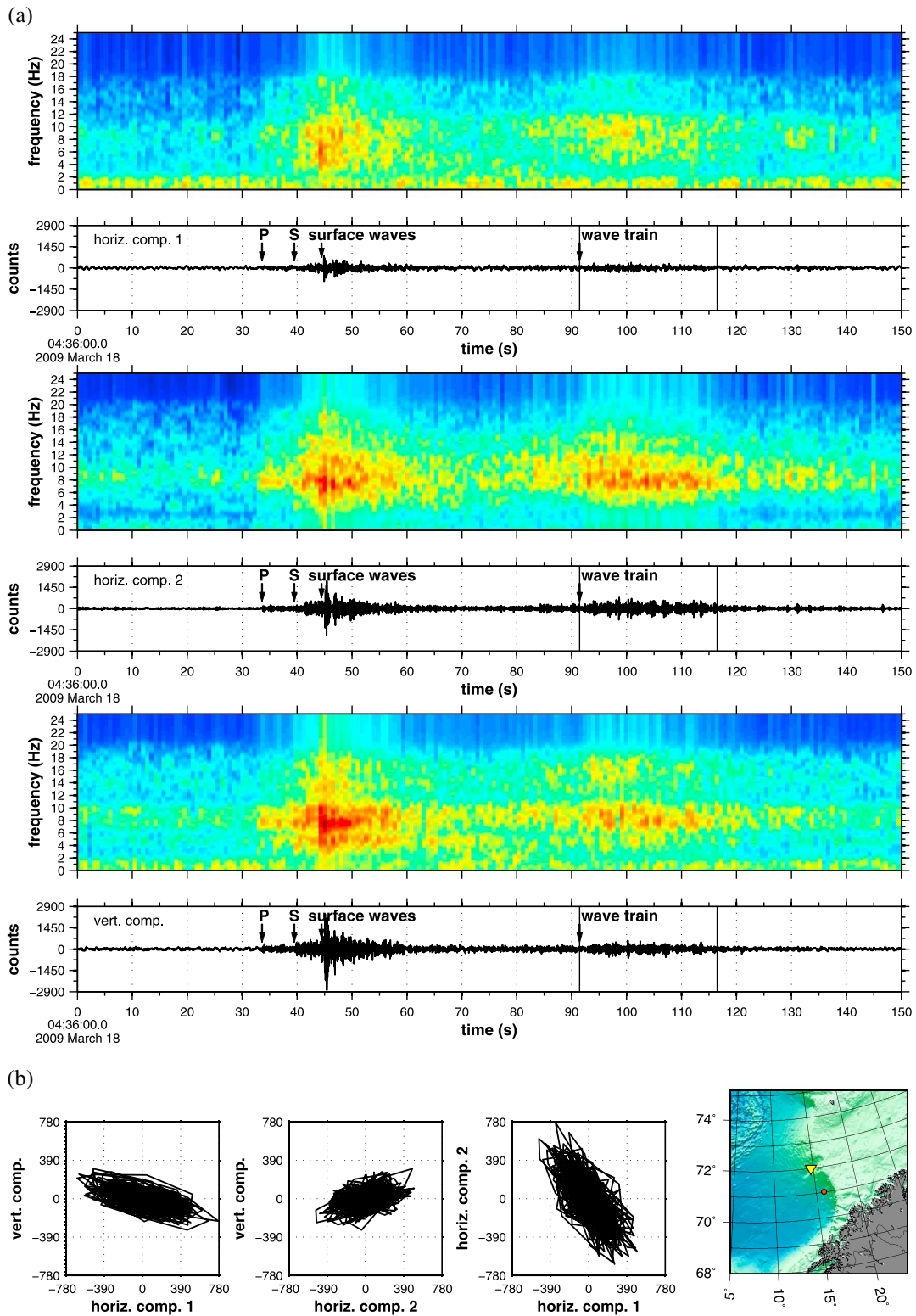


**Figure A2.** (a) Seismic records of earthquake no. 12 listed in Table A1 and corresponding spectrograms. Starting time of records corresponds to 18 March 2009, 04:36:00.0. Spectrograms are logarithmically scaled from minimum value of logarithm of amplitude (−0.7) to maximum value (2.9), where blue color corresponds to minimum and red to maximum. Spectrograms were calculated by sliding time windows of 1.5 s duration and 0.75 s overlap. Arrows indicate arrivals of *P*, *S*, and surface waves and occurrence of wave train following the earthquake. (b) Particle motion of wave train corresponding to the part of seismogram indicated in Figure A1a by vertical lines. Shown is particle motion in two vertical planes (vertical versus horizontal comp. 1, vertical versus horizontal comp. 2) and in a horizontal plane (horizontal comp. 2 versus horizontal comp. 1). Relative location of the earthquake epicenter and the HMMV is shown on the map.

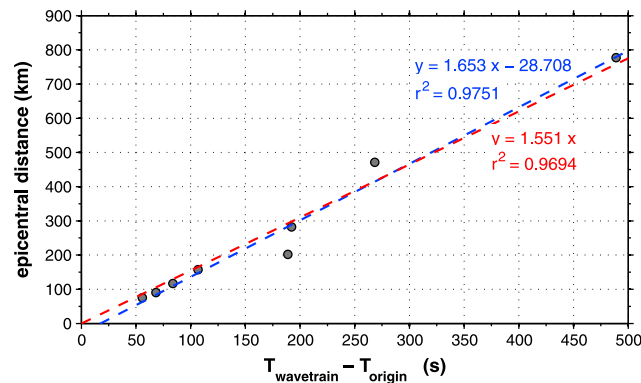


**Figure A3.** Difference between the origin times of identified earthquakes and the arrival times of wave trains plotted relative to epicentral distance (dots). Regression lines with parameters and correlation coefficient determined by least squares method in the case of linear fit (blue line) and linear fit at the assumption of zero interception (red line).

amplitudes and often concealed earthquake signals. These aspects may explain why most of the earthquakes from our list of events are not recognized in seismic records.

We determined spectral characteristics for all of the records for the 15 identified earthquakes. Figure A2a shows an example of a recorded earthquake with spectrograms for all three components of seismic motion. Amplitudes of *S* waves and surface waves are very well developed for most of the identified earthquakes for all components of seismic motion. Amplitudes of *P* waves in several cases are at the noise level, however it was possible to distinguish

them in spectrograms. Frequency content of seismic waves varies in the range of 5 Hz to 18 Hz.

For eight of the identified earthquakes on all three components of seismic motion we have observed particular wave trains after surface waves from earthquakes. The onset of these wave trains is very unclear because they show a gradual and very gentle amplitude increase and long duration. Their frequency content is in the same range as *S* waves and surface waves from earthquakes (see Figure A2a). Particle motion diagrams show that the wave trains are polarized mainly in the horizontal plane (Figure A2b), but due to unknown orientations of the horizontal components of the seismometer, their arrival azimuth was not determined. The wave trains occur 35–160 s after arrival of *S* waves. The difference between the arrival times of wave trains and the origin times of earthquakes is linearly increasing with epicentral distance (Figure A3). The least squares method at the assumption of zero interception of linear fit provides the speed of propagation of wave trains (1.55 km/s), which is very close to the speed of sound in water. Water depth of the HMMV (about 1300 m) falls into the depth range of the SOFAR channel, which is from 600 to 1800 m [Okal, 2001]. Thus, sources of late wave trains are most probably earthquakes, where late wave trains correspond to a *T* phase of seismic waves. Polarization and frequency content suggest a conversion of *T* waves to *S* waves in most cases of the identified earthquakes.

#### Acknowledgments

The work was supported by the EC funded European Sea Observatory NETWORK (EVK3-CT-2002-80008) and the Centre of Excellence: Arctic Gas Hydrate, Environment and Climate (CAGE) funded by the Norwegian Research Council (grant No. 223259). P. Franek is supported by a fellowship through the University of Tromsø. The seismic records of the OBS and data used to produce the results in this paper are available by contacting the authors. We thank T. Feseker (MARUM, Bremen, Germany) for helpful discussions and comments and Joel Johnson (University of New Hampshire, USA) for useful suggestions that improved the final version of the manuscript. We are also thankful to the crews and scientific parties of all LOOME-related cruises (R/V *Jan Mayen* 2008, R/V *Polarstern* 2009, R/V *Maria S. Merian* 2010), for deploying and recovering the OBS.

#### References

- Ader, T. J., and J.-P. Avouac (2013), Detecting periodicities and declustering in earthquake catalogs using the Schuster spectrum, application to Himalayan seismicity, *Earth Planet. Sci. Lett.*, *377*–378, 97–105, doi:10.1016/j.epsl.2013.06.032.
- Albarelo, D., M. Palo, and G. Martinelli (2012), Monitoring methane emission of mud volcanoes by seismic tremor measurements: A pilot study, *Nat. Hazards Earth Syst. Sci.*, *12*, 3617–3629, doi:10.5194/nhess-12-3617-2012.
- Bartosch, T., and D. Seidl (1999), Spectrogram analysis of selected tremor signals using short-time Fourier transform and continuous wavelet transform, *Ann. Geofis.*, *42*, 497–506.
- Beyer, A., R. Rathlau, and H. W. Schenke (2005), Multibeam bathymetry of the Håkon Mosby mud volcano, *Mar. Geophys. Res.*, *26*, 61–75, doi:10.1007/s11001-005-1131-8.
- Boles, J. R., J. F. Clark, I. Leifer, and L. Washburn (2001), Temporal variation in natural methane seep rate due to tides, Coal Oil Point area, California, *J. Geophys. Res.*, *106*, 27,077–27,086, doi:10.1029/2000JC000774.
- Déville, E., A. Battani, R. Griboulaud, S. Guerlais, J. P. Herbin, J. P. Houzay, C. Muller, and A. Prinzhofer (2003), The origin and processes of mud volcanism: New insights from Trinidad, in *Subsurface Sediment Mobilization*, vol. 216, edited by P. van Rensbergen et al., pp. 475–490, Geological Society of London, London, U. K.
- Díaz, J., J. Gallart, and O. Gasparà (2007), Atypical seismic signals at the Galicia Margin, North Atlantic Ocean, related to the resonance of subsurface fluid-filled cracks, *Tectonophysics*, *433*, 1–13, doi:10.1016/j.tecto.2007.01.004.
- Dimitrov, L. I. (2002), Mud volcanoes—The most important pathway for degassing deeply buried sediments, *Earth Sci. Rev.*, *59*, 49–76, doi:10.1016/S0012-8252(02)00069-7.
- Edy, C., H. Bisquay, and Shipboard Scientific Party (2004), Microbathymetry on ROV “Victor 6000”, in *The Expedition ARKTIS XIX/3 of the Research Vessel Polarstern in 2003*, Rep. Polar Mar. Res., vol. 488, edited by M. Klages et al., pp. 158–163, Alfred Wegener Institute for Polar and Marine Research, Bremerhaven, Germany.
- Egbert, G. D., and S. Y. Erofeeva (2002), Efficient inverse modeling of barotropic ocean tides, *J. Atmos. Oceanic Technol.*, *19*, 183–204, doi:10.1175/1520-0426(2002)019<0183:EIMOBO>2.0.CO;2.
- Embricaco, D., et al. (2013), Monitoring of gas and seismic energy release by multiparametric benthic observatory along the North Anatolian Fault in the Sea of Marmara (NW Turkey), *Geophys. J. Int.*, doi:10.1093/gji/ggt436.

- Feseker, T., J.-P. Foucher, and F. Harmegnies (2008), Fluid flow or mud eruptions? Sediment temperature distributions on Håkon Mosby mud volcano, SW Barents Sea slope, *Mar. Geol.*, *247*, 194–207, doi:10.1016/j.margeo.2007.09.005.
- Field, M. E., and A. E. Jennings (1987), Seafloor gas seeps triggered by a northern California earthquake, *Mar. Geol.*, *77*, 39–51, doi:10.1016/0025-3227(87)90082-X.
- Fischer, D., J. M. Mogollón, M. Strasser, T. Pape, G. Bohrmann, N. Fekete, V. Spiess, and S. Kasten (2013), Subduction zone earthquake as potential trigger of submarine hydrocarbon seepage, *Nat. Geosci.*, *6*, 647–651, doi:10.1038/ngeo1886.
- Flemings, P. B., X. Liu, and W. J. Winters (2003), Critical pressure and multiphase flow in Blake Ridge gas hydrates, *Geology*, *31*, 1057–1060.
- Foucher, J.-P., G. K. Westbrook, A. Boetius, S. Ceramicola, S. Dupré, J. Mascle, J. Mienert, O. Pfannkuche, C. Pierre, and D. Praeg (2009), Structure and drivers of cold seep ecosystems, *Oceanography*, *22*, 92–109.
- Ginsburg, G. D., A. V. Milkov, V. A. Soloviev, A. V. Egorov, G. A. Cherkashev, P. R. Vogt, K. Crane, T. D. Lorenson, and M. D. Khutorskoy (1999), Gas hydrate accumulation at the Håkon Mosby Mud Volcano, *Geo-Mar. Lett.*, *19*, 57–67, doi:10.1007/s003670050093.
- Halbach, P., E. Holzbecher, T. Reichel, and R. Moche (2004), Migration of the sulphate-methane reaction zone in marine sediments of the Sea of Marmara—Can this mechanism be tectonically induced?, *Chem. Geol.*, *205*, 73–82, doi:10.1016/j.chemgeo.2003.12.013.
- Hjelstuen, B. O., O. Eldholm, J. I. Faleide, and P. R. Vogt (1999), Regional setting of Håkon Mosby Mud Volcano, SW Barents Sea margin, *Geo-Mar. Lett.*, *19*, 22–28, doi:10.1007/s003670050089.
- Hornbach, M. J., D. M. Saffer, and W. Steven Holbrook (2004), Critically pressured free-gas reservoirs below gas-hydrate provinces, *Nature*, *427*, 142–144, doi:10.1038/nature02172.
- Huguenot, C., J. Mascle, E. Chaumillon, A. Kopf, J. Woodside, and T. Zitter (2004), Structural setting and tectonic control of mud volcanoes from the Central Mediterranean Ridge (Eastern Mediterranean), *Mar. Geol.*, *209*, 245–263, doi:10.1016/j.margeo.2004.05.002.
- Jerosch, K., M. Schlüter, J.-P. Foucher, A.-G. Allais, M. Klages, and C. Edy (2007), Spatial distribution of mud flows, chemoautotrophic communities, and biogeochemical habitats at Håkon Mosby Mud Volcano, *Mar. Geol.*, *243*, 1–17, doi:10.1016/j.margeo.2007.03.010.
- Kasahara, J. (2002), Tides, earthquakes, and volcanoes, *Science*, *297*, 348–349, doi:10.1126/science.1074601.
- Kennett, B. L. N., and E. R. Engdahl (1991), Traveltimes for global earthquake location and phase identification, *Geophys. J. Int.*, *105*, 429–465, doi:10.1111/j.1365-246X.1991.tb06724.x.
- Konstantinou, K. I., and V. Schlindwein (2002), Nature, wavefield properties and source mechanism of volcanic tremor: A review, *J. Volcanol. Geotherm. Res.*, *119*, 161–187, doi:10.1016/S0377-0273(02)00311-6.
- Kopf, A. J. (2002), Significance of mud volcanism, *Rev. Geophys.*, *40*(2), 1005, doi:10.1029/2000RG000093.
- Lapham, L., J. P. Chanton, C. S. Martens, P. D. Higley, H. W. Jannasch, and J. R. Woolsey (2008), Measuring temporal variability in pore-fluid chemistry to assess gas hydrate stability: Development of a continuous pore-fluid array, *Environ. Sci. Technol.*, *42*, 7368–7373, doi:10.1021/es801195m.
- Lapham, L., R. Wilson, M. Riedel, C. K. Paull, and M. E. Holmes (2013), Temporal variability of in situ methane concentrations in gas hydrate-bearing sediments near Bullseye Vent, Northern Cascadia Margin, *Geochem. Geophys. Geosyst.*, *14*, 2445–2459, doi:10.1002/ggge.20167.
- Leifer, I., and K. Wilson (2007), The tidal influence on oil and gas emissions from an abandoned oil well: Nearshore Summerland, California, *Mar. Pollut. Bull.*, *54*, 1495–1506, doi:10.1016/j.marpolbul.2007.03.014.
- Manga, M., M. Brumm, and M. L. Rudolph (2009), Earthquake triggering of mud volcanoes, *Mar. Petrol. Geol.*, *26*, 1785–1798, doi:10.1016/j.marpetgeo.2009.01.019.
- Michaut, C., Y. Ricard, D. Bercovici, and R. S. J. Sparks (2013), Eruption cyclicity at silicic volcanoes potentially caused by magmatic gas waves, *Nat. Geosci.*, *6*, 856–860, doi:10.1038/ngeo1928.
- Mienert, J., et al. (2009), 2008 Cruise report LOOME ESONET demonstration mission, *Esonews*, *3*, 1–7.
- Milkov, A. V. (2000), Worldwide distribution of submarine mud volcanoes and associated gas hydrates, *Mar. Geol.*, *167*, 29–42, doi:10.1016/S0025-3227(00)00022-0.
- Milkov, A. V. (2005), Global distribution of mud volcanoes and their significance in petroleum exploration as a source of methane in the atmosphere and hydrosphere and as a geohazard, in *Mud Volcanoes, Geodynamics and Seismicity*, vol. 51, edited by G. Martinelli and B. Panahi, pp. 29–34, Springer, Netherlands, doi:10.1007/1-4020-3204-8\_3.
- Milkov, A. V., P. R. Vogt, K. Crane, A. Y. Lein, R. Sassen, and G. A. Cherkashev (2004), Geological, geochemical, and microbial processes at the hydrate-bearing Håkon Mosby mud volcano: A review, *Chem. Geol.*, *205*, 347–366, doi:10.1016/j.chemgeo.2003.12.030.
- Neuberg, J. (2000), Characteristics and causes of shallow seismicity in andesite volcanoes, *Philos. Trans. R. Soc. London A*, *358*, 1533–1546, doi:10.1098/rsta.2000.0602.
- Niemann, H., and A. Boetius (2010), Mud volcanoes, in *Handbook of Hydrocarbon and Lipid Microbiology*, edited by K. N. Timmis, pp. 205–214, Springer, Berlin Heidelberg, doi:10.1007/978-3-540-77587-4\_13.
- Niemann, H., et al. (2006), Novel microbial communities of the Haakon Mosby mud volcano and their role as a methane sink, *Nature*, *443*, 854–858, doi:10.1038/nature05227.
- Okal, E. A. (2001), T-phase stations for the international monitoring system of the comprehensive nuclear-test ban treaty: A global perspective, *Seismol. Res. Lett.*, *72*, 186–196, doi:10.1785/gssrl.72.2.186.
- Okal, E. A. (2008), The generation of T waves by earthquakes, *Adv. Geophys.*, *49*, 1–65, doi:10.1016/S0065-2687(07)49001-X.
- Olofsson, B. (2010), Marine ambient seismic noise in the frequency range 1–10 Hz, *Leading Edge*, *29*, 418–435, doi:10.1190/1.3378306.
- Pape, T., T. Feseker, S. Kasten, D. Fischer, and G. Bohrmann (2011), Distribution and abundance of gas hydrates in near-surface deposits of the Håkon Mosby Mud Volcano, SW Barents Sea, *Geochem. Geophys. Geosyst.*, *12*, Q09009, doi:10.1029/2011GC003575.
- Perez-Garcia, C., T. Feseker, J. Mienert, and C. Berndt (2009), The Håkon Mosby mud volcano: 330 000 years of focused fluid flow activity at the SW Barents Sea slope, *Mar. Geol.*, *262*, 105–115, doi:10.1016/j.margeo.2009.03.022.
- Planke, S., H. Svensen, M. Hovland, D. A. Banks, and B. Jamtveit (2003), Mud and fluid migration in active mud volcanoes in Azerbaijan, *Geo-Mar. Lett.*, *23*, 258–268, doi:10.1007/s00367-003-0152-z.
- Pontoise, B., and Y. Hello (2002), Monochromatic infra-sound waves recorded offshore Ecuador: Possible evidence of methane release, *Terra Nova*, *14*, 425–435, doi:10.1046/j.1365-3121.2002.00437.x.
- Ripepe, M., E. Marchetti, C. Bonadonna, A. J. L. Harris, L. Pioli, and G. Ulivieri (2010), Monochromatic infrasonic tremor driven by persistent degassing and convection at Villarrica Volcano, Chile, *Geophys. Res. Lett.*, *37*, L15303, doi:10.1029/2010GL043516.
- Rudolph, M. L., and M. Manga (2012), Frequency dependence of mud volcano response to earthquakes, *Geophys. Res. Lett.*, *39*, L14303, doi:10.1029/2012GL052383.
- Sauter, E. J., S. I. Muyakshin, J.-L. Charlou, M. Schlüter, A. Boetius, K. Jerosch, E. Damm, J.-P. Foucher, and M. Klages (2006), Methane discharge from a deep-sea submarine mud volcano into the upper water column by gas hydrate-coated methane bubbles, *Earth Planet. Sci. Lett.*, *243*, 354–365, doi:10.1016/j.epsl.2006.01.041.

- Sultan, N., et al. (2011), Dynamics of fault-fluid-hydrate system around a shale-cored anticline in deepwater Nigeria, *J. Geophys. Res.*, *116*, B12110, doi:10.1029/2011JB008218.
- Talandier, J., and E. A. Okal (1996), Monochromatic T waves from underwater volcanoes in the Pacific ocean: Ringing witnesses to geyser processes?, *Bull. Seismol. Soc. Am.*, *86*, 1529–1544.
- Tary, J. B., L. Géli, C. Guennou, P. Henry, N. Sultan, N. Çağatay, and V. Vidal (2012), Microevents produced by gas migration and expulsion at the seabed: A study based on sea bottom recordings from the Sea of Marmara, *Geophys. J. Int.*, *190*, 993–1007, doi:10.1111/j.1365-246X.2012.05533.x.
- Tinivella, U., and M. Giustiniani (2012), An overview of mud volcanoes associated to gas hydrate system, in *Updates in Volcanology—New Advances in Understanding Volcanic Systems*, edited by K. Nemeth, pp. 225–267, InTech, Rijeka, Croatia, doi:10.5772/51270.
- Tolstoy, M., F. L. Vernon, J. A. Orcutt, and F. K. Wyatt (2002), Breathing of the seafloor: Tidal correlations of seismicity at Axial volcano, *Geology*, *30*, 503–506, doi:10.1130/0091-7613(2002)030<0503:BOTSTC>2.0.CO;2.
- Torres, M. E., J. McManus, D. E. Hammond, M. A. de Angelis, K. U. Heeschen, S. L. Colbert, M. D. Tryon, K. M. Brown, and E. Suess (2002), Fluid and chemical fluxes in and out of sediments hosting methane hydrate deposits on Hydrate Ridge, OR, I: Hydrological provinces, *Earth Planet. Sci. Lett.*, *201*, 525–540, doi:10.1016/S0012-821X(02)00733-1.
- Vogt, P. R., G. Cherkashev, G. Ginsburg, G. Ivanov, A. Milkov, K. Crane, A. Lein, E. Sundvor, N. Pimenov, and A. Egorov (1997), Haakon Mosby Mud Volcano provides unusual example of venting, *Eos Trans. AGU*, *78*, 549–557, doi:10.1029/97EO00326.
- Wang, H. F. (2000), *Theory of Linear Poroelasticity With Applications to Geomechanics and Hydrogeology*, Princeton Univ. Press, Princeton, N. J.